A phenomenological model for the responses of auditory-nerve fibers. II. Nonlinear tuning with a frequency glide

Qing Tan
Boston University Hearing Research Center, Department of Biomedical Engineering, Boston University, 44 Cummington Street, Boston, Massachusetts 02215

Laurel H. Carney[a)]
Boston University Hearing Research Center, Department of Biomedical Engineering, Boston University, 44 Cummington Street, Boston, Massachusetts 02215 and Department of Bioengineering and Neuroscience, Institute for Sensory Research, 621 Skytop Road, Syracuse University, Syracuse, New York 13244[b)]

(Received 31 December 2002; accepted for publication 22 July 2003)

A computational model was developed to simulate the responses of auditory-nerve (AN) fibers in cat. The model's signal path consisted of a time-varying bandpass filter; the bandwidth and gain of the signal path were controlled by a nonlinear feed-forward control path. This model produced realistic response features to several stimuli, including pure tones, two-tone combinations, wideband noise, and clicks. Instantaneous frequency glides in the reverse-correlation (revcor) function of the model's response to broadband noise were achieved by carefully restricting the locations of the poles and zeros of the bandpass filter. The pole locations were continuously varied as a function of time by the control signal to change the gain and bandwidth of the signal path, but the instantaneous frequency profile in the revcor function was independent of sound pressure level, consistent with physiological data. In addition, this model has other important properties, such as nonlinear compression, two-tone suppression, and reasonable Q_{10} values for tuning curves. The incorporation of both the level-independent frequency glide and the level-dependent compressive nonlinearity into a phenomenological model for the AN was the primary focus of this work. The ability of this model to process arbitrary sound inputs makes it a useful tool for studying peripheral auditory processing.
 [DOI: 10.1121/1.1608963]

PACS numbers: 43.64.Bt, 43.64.Pg [WJS]

I. INTRODUCTION

The auditory nerve (AN) transfers the information of sound stimuli from the cochlea to the cochlear nucleus, which projects to higher levels of the auditory nervous system. Detailed knowledge of the firing pattern of AN fibers is necessary to understand how sounds are encoded at the input stage of the auditory system. The goal of this study was to improve a previous nonlinear phenomenological model for the response patterns of AN fibers to different sound inputs. The computational AN model presented here includes the level-independent instantaneous frequency glide and the level-dependent compressive nonlinearity. These properties interact and influence both the rate and timing of AN responses. This model is a useful tool for the study of sound encoding in the peripheral auditory system, and it provides realistic responses that can be used as inputs to models of higher levels of the auditory system.

A system's impulse response can be estimated by the cross correlation of the response of the system to a wideband noise with the noise input waveform. This technique has been used as an indirect estimate of the basilar membrane (BM) impulse responses while the click response is a direct estimate (de Boer and Nuttall, 1997). The reverse-correlation (revcor) function is an extension of the cross-correlation method and is used as an indirect estimate of the AN impulse response (de Boer and de Jongh, 1978). A frequency modulation, or ''glide'' in the instantaneous frequency, has been reported in the impulse responses of BM (Robles *et al.*, 1976; de Boer and Nuttall, 1997; Recio *et al.*, 1997) and AN fibers (Lin and Guinan, 2000; Carney *et al.*, 1999). An upward frequency glide indicates that the early part of the impulse response is dominated by lower frequency components and the later part is dominated by higher frequency components (i.e., frequency increases as a function of time). A downward glide indicates the opposite trend (i.e., frequency decreases as a function of time).

Upward frequency glides were observed in BM and AN responses with relatively high characteristic frequencies (CF $>$1500 Hz), constant frequency glides were seen in AN fibers with medium CFs (CF=750–1500 Hz), and downward frequency glides were seen in low-CF AN fibers (CF$<$750 Hz) (Carney *et al.*, 1999). These frequency glides are consistent with the level-dependent peak-frequency shifts observed in auditory peripheral transfer functions [AN: Møller (1977); inner hair cell (IHC): Cheatham and Dallos (1999)]. Shera (2001a, b) explored instantaneous frequency glides in BM click responses and suggested that the slope of the normalized instantaneous frequency is independent of cochlear location for CFs above 1.5 kHz and strongly dependent on cochlear location for lower CFs.

The frequency glide pattern not only affects the fine

a)Author to whom correspondence should be addressed. Electronic mail: lacarney@syr.edu
b)Address for correspondence.

structure of AN responses in the time domain but also is related to the best-frequency[1] (BF) shift as a function of sound pressure level (SPL). This level-dependent BF shift can be qualitatively explained by the combination of the instantaneous frequency trend in the impulse response and the change in the shape of the impulse-response envelope at various input SPLs (Carney, 1999; Shera, 2001b). Due to the compressive nonlinearity, as SPL increases, the bandwidth of peripheral filters increases and the group delay of the filters decreases. Associated with the decreases in group delay is a shift of the envelope of the impulse response to smaller latencies. In fibers with CFs higher than 1500 Hz, the instantaneous frequency has an upward glide, which means that the beginning of the response has a relatively low instantaneous frequency. When the input SPL is increased, the group delay of the impulse response decreases; because earlier (lower-frequency) energy in the impulse response is emphasized as SPL increases, the best frequency at high SPLs decreases. For low-CF fibers, as SPL increases the group delay of the impulse response still decreases, but in this case the shift in the impulse-response envelope emphasizes the early (high-frequency) energy in the downward glide for the low-CF fiber. Therefore, the BF of low-CF fibers shifts upwards as the SPL increases. [See Fig. 1 in Carney (1999) for schematic diagram illustrating the inter relationship between the glide and the BF shift.]

An instantaneous-frequency glide in the impulse response of a filter is reflected in the asymmetry of its transfer function. This asymmetry indicates that there are poles with different damping coefficients within the filter. The difference in damping coefficients is associated with the frequency glide in the filter's impulse response (see below for more detail). Because the middle ear affects the asymmetry of cochlear filters (Cheatham and Dallos, 2001), a simple middle-ear function consisting of a linear band-pass filter (Rosowski, 1996) was used to model this aspect of the frequency glide. The contribution of the middle-ear filter to the frequency glide is most important at low CFs.

One goal of this study was to simulate the frequency-glide phenomenon in the AN fiber's impulse response. Another focus was the inclusion of the compressive nonlinearity, which is the decrease in the gain of the BM response for mid- to high-level sound inputs (Rhode, 1971; Ruggero *et al.*, 1997). The compressive nonlinearity causes broadened tuning of AN responses and shifted phase responses with increased SPLs. Two-tone suppression, which is the reduction of the response to a tone at CF when a second tone is presented at a frequency other than CF, is associated with the compressive nonlinearity (Ruggero and Rich, 1991).

Recent reports of phenomenological AN models have focused on various aspects of fiber responses. The responses of the auditory periphery, whether recorded from single AN fibers or single sites on the basilar membrane, are characterized as level-dependent bandpass filters. A nonlinear AN model that was developed by Carney (1993) and extended by Zhang *et al.* (2001) and Heinz *et al.* (2001c) includes a fourth-order gamma-tone filter with level-dependent bandwidth and gain. The most recent versions of this model included level-dependent phase responses, compression, and two-tone suppression; however, the frequency glide observed by Carney *et al.* (1999) in the reverse-correlation (revcor) functions of cat AN fibers was not included.

Meddis and colleagues' (2001) BM model consists of a dual resonance nonlinear (DRNL) filter with two parallel branches, one linear and the other nonlinear. This model and Goldstein's (1990, 1995) multiple bandpass nonlinear (MBNL) model are extensions of Pfeiffer's (1970) bandpass nonlinear (BPNL) model. These models successfully reproduce many physiological phenomena related to basilar membrane motion. However, they do not address the level independence of the instantaneous-frequency glide, which is a focus of the study presented here. Meddis *et al.* (2001) qualitatively describe the instantaneous-frequency glide in the impulse response of their model, but they do not quantify the frequency glide or demonstrate its level independence. The level dependency of this instantaneous frequency in the impulse response of the DRNL model will be compared to that of the model presented here.

Irino and Patterson (1997, 2001) proposed a gammachirp auditory filter to account for peripheral auditory processing. The gammachirp filter is an extension of the gammatone filter and was the first model to include the frequency glide property in its impulse response. Although this model includes frequency glides in the impulse responses, the trends of the BF shifts as a function of SPL in Irino and Patterson's (2001) model are not consistent with physiological data. The response areas of Anderson *et al.* (1971, their Fig. 8) and the revcor filters of Møller (1977), Evans (1977), and de Boer and de Jongh (1978) had monotonic shifts in BF to lower frequencies with increased SPLs for fibers with high CF. However, the BF of one example in Irino and Patterson (2001, their Fig. 7) shifts to higher frequencies for mid-level sounds and back to lower frequencies for high-level sounds. The BF of another example (their Fig. 10, CF=1800 Hz) shifts to higher frequencies with increased SPLs. An accurate representation of the level-dependent shifts in BF was one of the focuses of the model presented here, as it is associated with the frequency glide.

Robert and Eriksson's (1999) cochlear model is based on a filter bank of all-pole gamma-tone filters (APGFs). Each branch of the filter bank consists of a passive and an active (nonlinear) bandpass filter in series. These two filters are tuned to different center frequencies, and, therefore, a BF shift can be observed when input SPL changes. This level dependency of BF suggests that their filter-bank model may have an instantaneous frequency glide in the impulse response. However, Robert and Eriksson (1999) did not show the instantaneous frequency profile or test its level independence. In addition, Robert and Eriksson's (1999) gammatone filters do not include any zeros, which are important for producing downward instantaneous-frequency glides (see Sec. II for detail). These downward glides are observed in low-CF AN fibers (Carney *et al.*, 1999).

de Boer and Nuttall (2000) also investigated the instantaneous-frequency glide in the response of the basal BM in a modeling study based on the EQ-NL theorem (de Boer, 1997). In their model, the impedance of the BM is described by two linear components, with a signal level-

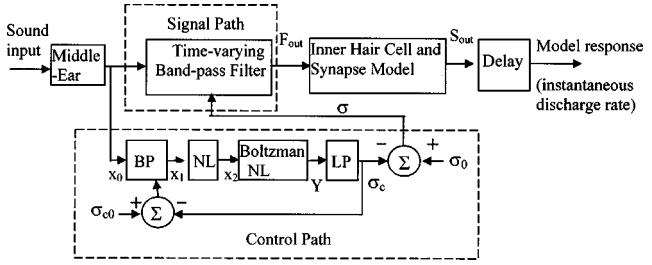

FIG. 1. Schematic diagram of the AN model. The model included a middle-ear model, a signal path, a control path, the IHC and synapse model, and a time delay. See text for more detail.

dependent coefficient that introduces the level dependence of bandwidth, gain, and peak frequency of the BM response in the frequency domain, along with the level-invariance of the glide in the impulse response. They only modeled responses in the base, and thus their model only described an upward frequency glide, but the general approach could be adapted to describe the downward glide at low frequencies. Their level-dependent coefficient varied the relative contributions of the two impedances; this coefficient did not vary with time, but was set to a single value to explain responses at a fixed stimulus noise level. The level-dependent parameter in the de Boer and Nuttall (2000) study plays a similar role in their model as the output of the control path in the model presented here. However, in the model described here, the parameter that controls the tuning at the level of the BM is both time and level dependent. The temporal variation of the nonlinearity is presumably more important at low frequencies because the dynamics of the compressive nonlinearity are fast enough that the properties of the system vary within a stimulus period at low frequencies. In addition, using a time-dependent coefficient to control the nonlinear system allows the model to be applied to a broader range of complex stimuli.

The present study combined the level-independent frequency glide with level-dependent features (e.g., the gain and bandwidth of peripheral tuning) in a simple manner to create a model that can process arbitrary stimuli. Previous studies (Shekhter and Carney, 1997; Tan and Carney, 1999) showed that careful selection of the locations of poles and zeros in the complex plane made it possible to design filters with realistic instantaneous frequency glides in the impulse responses of the filter. The model described here extended the model of Tan and Carney (1999) by combining the pole-zero approach with a feed-forward control path, thereby modeling the compressive nonlinearity of the auditory periphery.

II. MODEL DESCRIPTION

A. Model overview

The basic model components are shown in the block diagram in Fig. 1. The model consisted of four parts: a middle-ear model, a time-varying bandpass filter as the signal path, a nonlinear control path, and an IHC and synapse model.[2] The middle-ear model was a linear bandpass filter based on the middle-ear frequency response properties described by Rosowski (1996). This linear bandpass filter had two pairs of poles and one second-order zero in control space. The locations of the poles and zeros are specified in Table I. The low-frequency zeros of the middle-ear filter improved the downward frequency glide in the model's impulse response at low CFs.

Basilar membrane tuning was modeled with a time-varying bandpass filter, and the compressive nonlinearity of the BM was achieved with the nonlinear control path. The IHC and synapse model was based on that in Zhang *et al.* (2001). A 0.5-ms delay was added to the model output to match model and neural latencies. The output of this model was the instantaneous firing rate as a function of time.

This section describes the major components of the signal path and the control path of the model. This is followed by a description of how the parameters for model fibers across a range of CFs were estimated from AN recordings. The values of all model parameters are listed in Table I.

B. The signal path

The signal path was configured to produce a frequency glide in its impulse response. To illustrate mathematically how manipulation of pole-zero locations generates frequency glides in impulse responses, we consider a fourth-order linear filter with two complex-conjugate pole pairs[3] at $p_1(-x_1,2\pi f_1)$, $p_2(-x_2,-2\pi f_1)$, $p_3(-x_1,2\pi f_2)$, and $p_4(-x_2,-2\pi f_2)$, where $x_1>0$ and $x_2>0$. The transfer function of this simplified linear filter is

$$H(s)=\frac{a}{(s-p_1)(s-p_2)(s-p_3)(s-p_4)}. \tag{1}$$

The right side of Eq. (1) can be transformed into the sum of four first-order fractions:

$$H(s)=\frac{a_1}{(s-p_1)}+\frac{-a_1}{(s-p_2)}+\frac{a_2}{(s-p_3)}+\frac{-a_2}{(s-p_4)}, \tag{2}$$

where a_1 and a_2 are gains derived by factoring the right side of Eq. (1).

In the time domain, the impulse response of this linear filter [the inverse Laplace transform of Eq. (2)] is

$$h(t)=2a_1e^{-x_1t}\sin(2\pi f_1t) + 2a_2e^{-x_2t}\sin(2\pi f_2t), \quad \text{for } t\geqslant 0; \tag{3}$$

x_1 and x_2 determine how quickly the envelopes of the first and second terms in Eq. (3) reach their peak values, respectively. If it is assumed that $x_1>x_2$ and the values of a_1 and a_2 are carefully adjusted ($a_1>a_2$), then the first term has a larger amplitude and dominates at the beginning of the impulse response $h(t)$. The second term dominates the latter part of $h(t)$ because the first term decays faster than the second term. Thus, the instantaneous frequency is closer to f_1 at the beginning of the impulse response and is closer to f_2 at the end of the impulse response. Addition of poles to the filter provides increased control over the frequency shifts as a function of time in $h(t)$.

A fifth-order zero was placed on the real axis in the complex plane. For lower CFs, the zero is pushed closer to

TABLE I. Parameter values.

Parameter CF	Description Characteristic frequency	Value
Middle ear model		
Pm1_real	Real part of pole 1 in middle ear model (Hz)	−250
Pm1_img	Imaginary part of pole 1 in middle ear model (Hz)	400
Pm2_real	Real part of pole 2 in middle ear model (Hz)	−2000
Pm2_img	Imaginary part of pole 2 in middle ear model (Hz)	6000
Zm	Location of the zero on real axis for middle ear model (rad/s)	−200
Control path		
F_{cwb}	Center frequency of the wide-band filter (Hz)	1.2 mm basal to fiber CF
BW_{wb}	Bandwidth of the wide-band filter (Hz)	CF/4
Acp	Parameter in the first nonlinear function	100
Bcp	Parameter in the first nonlinear function	2.5
Ccp	Parameter in the first nonlinear function	0.6
S_0	Parameter in the second nonlinear function	8.0
S_1	Parameter in the second nonlinear function	3.0
T_0	Parameter in the second nonlinear function	0.85
T_1	Parameter in the second nonlinear function	5.0
Fclp	Cut-off frequency of the low-pass filter (Hz)	800
G_{control}	Gain in control path	See Eq. (18)
σ_c	Output of the control path	
Signal path		
P_a	Relative locations of poles, real part in the bandpath filter of the signal path	See Eq. (9)
P_b	Relative locations of poles, imaginary part	See Eq. (10)
P_ω	Imaginary part of the pole closest to the imaginary axis	See Eq. (12)
σ	Real part of the pole closest to the imaginary axis	$\sigma=\sigma_0-\sigma_c$
σ_0	Real part of the pole closest to the imaginary axis at quiet	See Eq. (11)
Z_0	Parameter for the location of the zeros in signal path	0.9
Z_1	Parameter for the location of the zeros in signal path	−1.5
Inner hair cell and synapse model See Zhang *et al.* (2001)		

the origin, which makes the low-frequency side of the filter transfer function steeper and the high-frequency side shallower than that for high CFs.

The combined influence of zeros and poles on the frequency glide can be illustrated as follows: For a simple system with one pair of poles (in conjugate) and one zero on the negative real axis

$$H(s)=\frac{(s+c)}{(s+a)^2+b^2}. \tag{4}$$

For the convenience of the inverse Laplace transform, Eq. (4) can be rewritten as

$$H(s)=\frac{(s+a)}{(s+a)^2+b^2}+\frac{(c-a)}{(s+a)^2+b^2}. \tag{5}$$

In the time domain, the impulse response is

$$h(t)=e^{-at}\left[\cos(bt)+\frac{(c-a)}{b}\sin(bt)\right], \quad \text{for } t\geqslant 0, \tag{6}$$

or, more conveniently,

$$h(t)=e^{-at}\sqrt{1+\left(\frac{(c-a)}{b}\right)^2}\cos\left(bt-\arctan\left(\frac{(c-a)}{b}\right)\right), \quad \text{for } t\geqslant 0. \tag{7}$$

For a slightly more complicated system with two pairs of poles and two zeros, as shown in Fig. 2, the poles and zeros can be divided into two groups, each having one zero and one pair of conjugate poles. The location of the zeros affects the coefficient in Eq. (7).

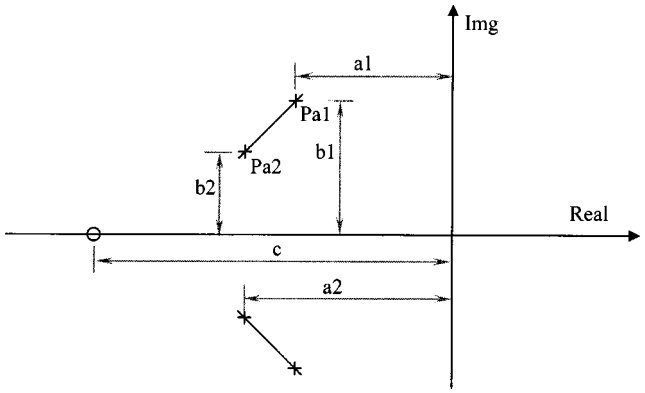

FIG. 2. A simple example of pole-zero locations for a bandpass filter, which has two pairs of poles (P_{a1}/P_{a2} and their conjugates) and one zero (z) in control space. The relative locations of the poles and zeros affect the trend of the instantaneous frequency profile in the filter's impulse response. In this example, P_{a2} has a larger damping coefficient and smaller resonance frequency than P_{a1} does. Therefore, the beginning part of the impulse response is dominated by relatively lower frequency (b_2) and the later part is dominated by higher frequency (b_1).

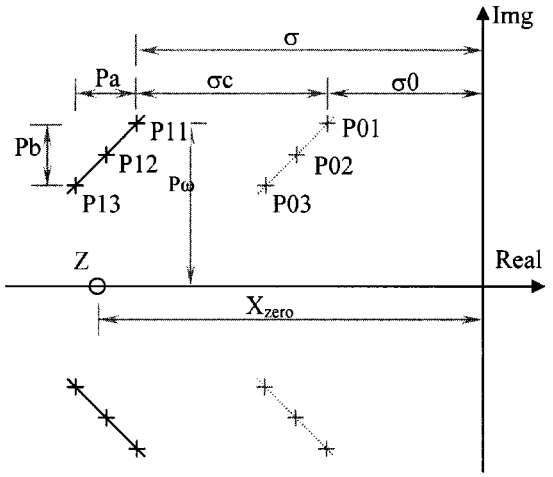

FIG. 3. Pole-zero locations for the bandpass filter in the model's signal path. Ten pairs of poles (P11 and P13 were fourth-order poles and P12 was a second-order pole) and a tenth-order zero were included. P01, P02, and P03 are the pole locations when the input sound intensity is zero for the poles P11, P12, and P13, respectively.

The envelope ratio between the two groups of poles and zeros, i.e.,

$$R=\frac{e^{-a_1 t}\sqrt{1+((c-a_1)/b_1)^2}}{e^{-a_2 t}\sqrt{1+((c-a_2)/b_2)^2}}, \tag{8}$$

determines the relative dominance of each group of poles when determining the instantaneous frequency at time t.

The model presented here had ten pairs of conjugate poles. The relative locations of the poles and the locations of ten zeros determined the instantaneous frequency glide (Fig. 3). The locations of the poles and zeros were set to be functions of model CF based on fitting revcor functions for a population of AN fibers, as described later. The model-CF dependence of the pole locations is described as

$$\log_{10}(P_a)=\log_{10}(\mathrm{CF})\times 1.0230+0.1607; \tag{9}$$

$$\log_{10}(P_b+1000)=\log_{10}(\mathrm{CF})\times 1.4292-1.1550; \tag{10}$$

$$\log_{10}(\sigma_0)=\log_{10}(\mathrm{CF})\times 0.4+1.9; \tag{11}$$

$$P_\omega=1.0854\times\mathrm{CF}-106.0034; \tag{12}$$

where P_a specifies the relative real parts of the poles, P_b specifies the relative imaginary parts of the poles, and P_ω is the imaginary part of the pole closest to the imaginary axis (see Fig. 3). All zeros were at the same location on the real axis, X_{zero}. The distance between the zeros and the origin was a function of CF on a log-log scale:

$$\log_{10}(X_{\mathrm{zero}})=Z_1\log_{10}(\mathrm{CF})+Z_0. \tag{13}$$

The zeros move away from the origin to negative infinity as CF increases. This definition of X_{zero} emphasizes the dominance of the poles with higher frequency at the beginning of the impulse response, especially for low CFs.

The signal-path filter had two eighth-order poles and one fourth-order pole, their complex conjugates, and a tenth-order zero on the real axis. This was the minimum number of poles and zeros required to generate realistic frequency glides in the time domain and realistic sharpness of tuning in the frequency domain.

C. The control path

The compressive nonlinearity is an important property of cochlear tuning in the healthy ear. This property was achieved by including the control path, which continuously changed the bandwidth and gain of the signal path. The control path included four segments in series (Fig. 1).

A nonlinear wideband filter determined the frequency range of the stimulus that affects the bandwidth and gain of the signal path. The bandwidth of the control-path wideband filter was set to twice the bandwidth of the signal path when there was no input signal. The center frequency of the wideband filter was set to a frequency corresponding to the place on the BM approximately 1.2 mm basal to the place that corresponded to the model CF. The bandwidth and the basal shift of the control path were chosen to achieve the appropriate shape of AN suppression tuning curves (e.g., Sachs and Kiang, 1968; Arthur *et al.*, 1970; Delgutte, 1990). The gain of the wideband filter was normalized to one at the model CF. A feedback signal derived from the output of the control path increased the bandwidth of the wideband filter with larger input sound intensity. This bandwidth control and the normalization of the gain resulted in different slopes in the two-tone suppression growth functions for suppressor frequencies above or below model CF (see below, Fig. 13).

A symmetric nonlinear function adopted from Zhang *et al.* (2001) followed the wideband filter:

$$X_2(t)=\mathrm{sgn}[X_1(t)]B_{cp}\log(1+A_{cp}|X_1(t)|^{Ccp}). \tag{14}$$

In Eq. (14), $X_1(t)$ is the output of the wideband filter in Pascals and $X_2(t)$ is the output of the symmetric nonlinear function. This compressive function made it easier to control the shape of the BM velocity-intensity function (see below, Fig. 7).

An asymmetric second-order Boltzmann function followed the symmetric logarithmic nonlinear function. This Boltzmann function corresponded to the membrane potential-displacement function of the outer hair cell, as suggested by Mountain and Hubbard (1996):

$$Y[X_2(t)]=B[X_2(t)]-B(0), \tag{15}$$

where x_2 was the output of the asymmetric function described by Eq. (14), and $B(x)$ was the second-order Boltzmann function:

$$B[x(t)]=\frac{1}{1+\exp[(T_0-x(t))/S_0]\times(1+\exp[(T_1-x(t))/S_1])}. \tag{16}$$

$B(0)$ was subtracted from $B[x(t)]$ to guarantee that $Y(0)$ was zero.

The parameters T_0, T_1, S_0, and S_1 were chosen such that the asymmetry of this control-path nonlinearity had a 7:1 ratio, as suggested by the responses of outer hair cells (OHCs) (Mountain and Hubbard, 1996).

The last component of the control path was a second-order low-pass filter with an 800-Hz cutoff frequency. The cutoff frequency of this filter was estimated from the results of Recio *et al.* (1998), which showed that the time course of the onset of compression has a time constant of approximately 0.2 ms, which corresponds to an 800-Hz cutoff frequency. This filter was chosen to be second order for simplicity; the effect of filter order will be explored in future work.

The control signal (the output of the control path), $\sigma_c(t)$, changes the real part of the locations of the poles of the band pass filter in control space [i.e., a positive $\sigma_c(t)$ makes the pole locations move further away from the imaginary axis and a negative $\sigma_c(t)$ makes the pole locations move closer to the imaginary axis]:

$$\sigma_i(t) = \sigma_{i0} - \sigma_c(t), \tag{17}$$

where $\sigma_i(t)$ is the damping coefficient of the ith pole, σ_{i0} is the damping coefficient of the ith pole when the input is zero, and $\sigma_c(t)$ is the control signal. Note that $\sigma(t)$ in Fig. 1 is a vector representing the real parts of all of the poles. The vector σ_0 contains the values of σ when no stimulus is present.

D. The IHC and synapse model

The IHC and synapse models were the same as in Zhang *et al.* (2001). The IHC model consisted of a logarithmic saturating function followed by a seventh-order low-pass filter. The IHC-AN synapse model was a time-varying three-store diffusion model [Westerman and Smith (1988); adapted into a time-varying model by Carney (1993) and Zhang *et al.* (2001)]. The model described here included only AN fibers with high spontaneous rates.

E. Parameter estimation

The relative positions of the poles in the signal path (P_a and P_b in Fig. 3) were estimated by fitting the model response to revcor functions of low-frequency cat AN fibers (Carney and Yin, 1988). The damping coefficient of the poles, σ_{80} (the average value of σ for responses to an 80-dB SPL noise), was initially estimated on the basis of cat revcor functions computed for AN responses to 80-dB SPL (rms) noise stimuli. Using 80-dB SPL responses for the initial parameter estimation had two advantages over using lower-level data. First, when the input SPL is high, the signal-to-noise ratio in the revcor function is relatively high. Second, revcor functions for 80-dB SPL responses were available for most fibers in the data set used (Carney and Yin, 1988). A linearized model (with the control signal set to zero and thus with level-independent pole locations) was first used to fit the 80-dB SPL revcor functions. The imaginary part of the pole that was closest to the imaginary axis was first set to the peak frequency of the revcor function's magnitude spectrum. The Marquardt (1963) method was then used to estimate the locations of the poles and zeros in the control space. For simplicity, the zeros were set so that they were always on the real axis. The target function of the parameter estimation was to minimize the rms value of the difference between revcor data and model revcor functions. Several values were tested as the initial imaginary part of the pole closest to the imaginary axis so that the fitting performance would not be limited by chance selection of a value.

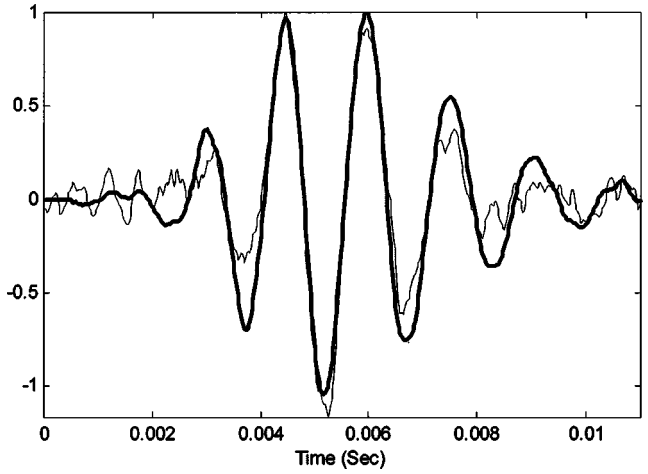

FIG. 4. An example of the model revcor fitted to cat data. The thin line is a revcor function from cat [unit 15 from cat 86166 (Carney *et al.*, 1999)] and the bold line is the corresponding model result. The CF of this fiber is 650 Hz. A downward frequency glide is apparent in these impulse responses, as the zero crossings are increasingly separated at later times in the responses.

An example of optimized locations for poles and zeros is shown in Fig. 3. (The poles for the high-SPL filter are on the solid short line and are P11, P12, and P13) The parameters estimated with the high-level AN revcor functions were P_a, P_b, P_ω and σ_{80}, where P_a and P_b were the relative positions of the poles as illustrated in Fig. 3; P_ω was the imaginary part of the pole with the largest imaginary part; and σ_{80} was the real part of the poles with the largest imaginary part and corresponds to the average value of σ when the stimulus is white noise at 80 dB SPL. Figure 4 shows an example of a model revcor function fit to cat revcor data [fiber U15-C86166 from Carney *et al.* (1999)]. This AN fiber with CF of 650 Hz has a downward frequency glide in its impulse response.

Revcor data (Carney and Yin, 1988) are available mostly for high SPLs (>40 dB SPL), which makes it difficult to estimate the tuning properties of AN fiber for low SPLs for a wide CF range based on revcor data (Carney and Yin, 1988). Q_{10} data (Miller *et al.*, 1997) are based on the threshold tuning curves of AN fiber responses. Thus Q_{10} data can be used to estimate the tuning properties of AN fibers at low SPLs. The Q_{10} data set was used to determine the locations of the poles in the resting state (when there was no sound input), specifically the value of σ_0 (σ in quiet). The CF-dependent gain of the control signal, G_{control} was adjusted such that an input of 80-dB SPL noise resulted in an average control signal equal to the difference in the real parts of P_{11} and P_{01}. The Q_{10} value was then measured for the nonlinear model, and P_{01}, P_{02}, P_{03}, and the gain of the control signal were adjusted until the model's Q_{10} value matched experimental Q_{10} data for the fiber's CF. After σ_0 and σ_{80} were set as functions of CF, the control signal was adjusted to produce an appropriate value to control the locations of the poles in

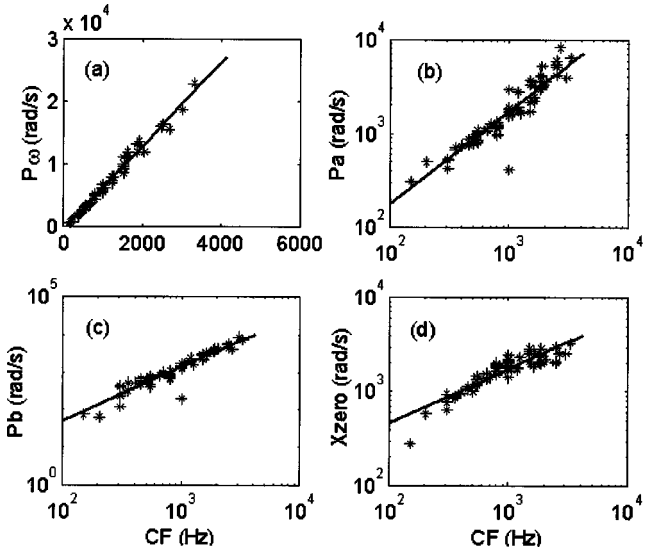

FIG. 5. Parameter estimation results for the pole and zero locations in the signal path for (a) P_ω, (b) P_a, (c) P_b, and (d) X_{zero} (see Fig. 3 for a description of the parameters). Parameter values fit to each fiber's revcor function are shown as stars. Simple expressions for each of the parameters, illustrated by the black lines, were set up and fit to the population results.

quiet and in 80-dB SPL noise. The CF-dependent gain was described by the following equation:

$$G_{\text{control}} = \frac{10^{0.5732CF+1.522} - 10^{0.4CF+1.9}}{0.3357}. \tag{18}$$

The parameter fits for the entire set of fibers were pooled for each parameter (Fig. 5). Simple expressions for the values of these parameters were established as functions of CF, as shown in the text above [Eqs. (9)–(13)], enabling the model to simulate AN fiber responses for any CF up to approximately 3500 Hz. The CF range was limited by the reduction in quality of revcor functions for high CF fibers (Carney and Yin, 1988). A total of 139 cat AN revcor functions from Carney and Yin (1988) were used for parameter estimation. In Fig. 5(a), it is clear that P_ω, the imaginary part (i.e., frequency) of the pole closest to the imaginary axis, is simply related to CF, as expected. P_a and P_b [Figs. 5(b) and (c)] are differences in the real and imaginary parts, respectively, of the poles at each CF (as illustrated in Fig. 3). Figure 5(d) shows the distance of the zeroes from the origin along the negative real axis (note that this is plotted as a positive distance, so that log axes can be used.) Appendix A provides CF-dependent model parameter values for three example CFs, one low-CF fiber with a downward glide, one with CF=1000 Hz which has essentially no glide, and one high-CF fiber with an upward glide.

III. RESULTS

This section illustrates several response properties of the model to tones and other stimuli. It begins with a description of the model's frequency glide, since that was the primary goal in the development of this model. Other fundamental response properties to tones at CF and to other stimuli are then shown. Nonlinear aspects of average rate and temporal response properties were of particular interest and are discussed below.

A. Instantaneous frequency glide

The primary goal of this effort was to incorporate a glide in the instantaneous frequency (IF) of the model's impulse response. The IF glide in this model's revcor function was very close to that reported in the data. An important feature of the IF glide is the constant slope at different noise levels. The model possesses this property because the relative positions of the poles do not change at different sound intensities (i.e., all the poles move in the same direction and have the same amount of displacement). Since the IF glide is determined by the relative positions of the poles, this model had a level-independent IF profile in its revcor function.

Figure 6(a) shows revcor functions for an AN fiber with CF equal to 2060 Hz at six noise levels from 30 to 80 dB SPL, alongside model revcor functions for a fiber with the same CF [Fig. 6(b)]. The zero-crossing points of the revcor functions were almost identical at different SPLs (as indicated by the vertical dotted lines) throughout the timecourse of the revcor functions; therefore, the revcor function's instantaneous frequency is independent of input SPL. Figures 6(c) and (d) show the instantaneous-frequency profiles for three AN fibers (CF=2500, 1600, and 550 Hz from top to bottom), at three levels (40, 60, and 80 dB SPL), alongside instantaneous-frequency profiles for three model AN fibers with the same CFs. To calculate the IF of a revcor function, the envelope of the revcor function was calculated by taking the absolute value of the Hilbert transform of the revcor function. IF was then calculated over the time period where the envelope was more than one quarter of the peak value, using the zero-crossing method (see Appendix B for details about calculation of instantaneous frequency). The overlap of the IF trajectories for the same revcor function at different levels verified the level independence of IF. Generally, the slopes of the IF trajectories increased as a function of CF. The slopes were usually positive (upward) for CFs greater than 1.5 kHz and were negative (downward) for CFs less than 0.75 kHz (Carney *et al.*, 1999). For the same AN fiber, or for the model at the same CF, the duration of the IF trajectory was shorter at higher levels because the time duration of the revcor function was shorter at higher levels [Figs. 6(a) and (b)]. This phenomenon reflects the increasing bandwidth of the revcor function at higher levels due to the compressive nonlinearity. Note that the model revcor functions have longer duration impulse responses than this particular example fiber [Figs. 6(a) and (b)]; this reflects the fact that the tuning for the model, which was based on Q_{10} values for a large population of fibers, was slightly sharper than the tuning for this particular fiber.

B. Rate-level curves

At low sound intensity, the control signal of this model was small (i.e., σ_c is almost zero and σ is near σ_0), and the filter in the signal path behaved like a linear bandpass filter with relatively narrow bandwidth and high gain. The filter output was compressed by the nonlinear control mechanism

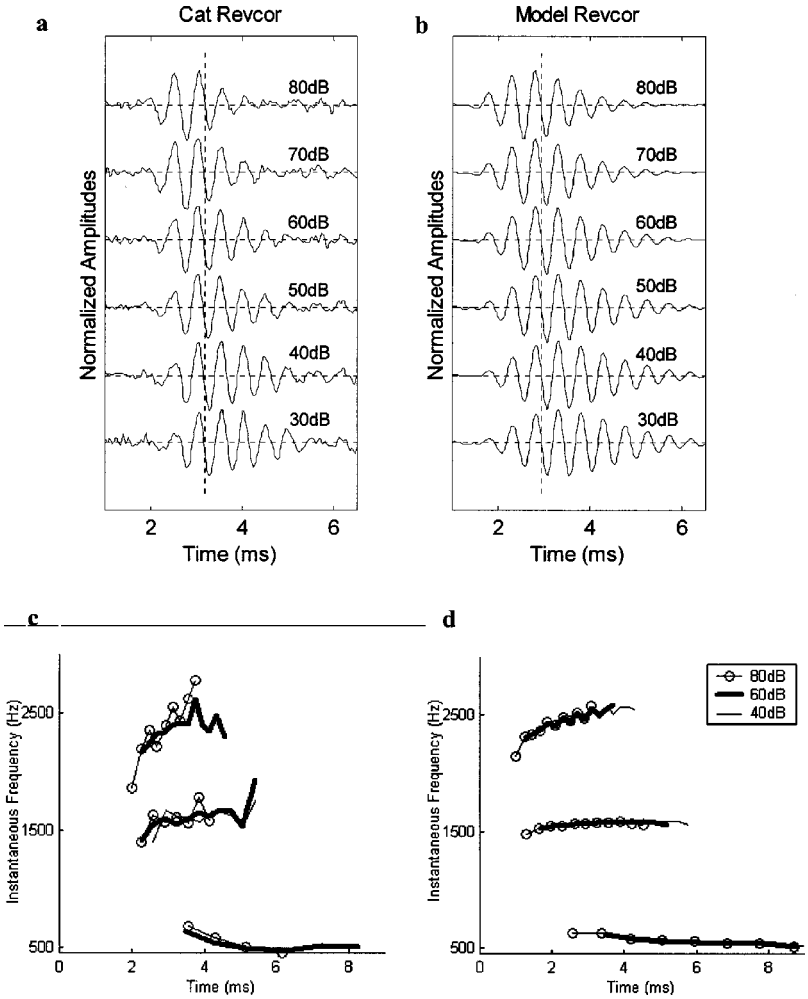

FIG. 6. Revcor functions and instantaneous-frequency profiles. (a) Measured revcor functions for AN fiber with CF=2060 Hz at six levels (30 to 80 dB SPL) (unit 86100-25 from Carney and Yin, 1988), (b) Model revcor functions for a fiber with matching CF. All revcor functions were normalized to their peak amplitude. (c) Measured AN instantaneous-frequency glides calculated based on zero-crossings from revcor functions. These examples show overlying instantaneous-frequency profiles computed from responses to 40, 60, and 80 dB SPL noise stimuli. CFs were 550 Hz (unit 86100-26), 1600 Hz (86100-7), and 2500 Hz (86100-2). (d) Model AN instantaneous-frequency profiles for fibers with CFs matched to the measured fibers. The overlap of the measured and model instantaneous-frequency profiles for different levels indicates that the instantaneous-frequency glides are level independent.

(i.e., σ_c and σ are larger than their values corresponding to sound intensity below threshold) when CF-tone levels were greater than 20 dB SPL. At very high SPLs, the control signal was nearly saturated, which made the filter output behave more linearly.

The compressive nonlinearity is illustrated in Fig. 7, which shows the root mean square (rms) value of the signal path output (F_{out} in Fig. 1) as a function of the input sound pressure level for several CFs. The input is a 50-ms duration pure tone at the model's CF with 2.5-ms onset and offset times. The compressive nonlinearity is stronger for higher CFs (Rhode and Cooper, 1996; Ruggero *et al.*, 1997). Figure 8 illustrates (a) the level-dependent onset rate, (b) sustained rate, and (c) synchronization coefficient of the model's responses to a pure tone at CF. (The left and right columns are results for model CFs at 1100 and 4000 Hz, respectively.) Both the onset rate and the sustained rate increase as the input SPL increases. The dynamic range of the onset rate is larger than that of the sustained rate (about 40 dB), which is appropriate for AN fibers (Smith, 1988).

C. Tuning curves and Q_{10} values

Tuning curves represent the excitation threshold of an AN fiber to tones at different frequencies (Kiang *et al.*, 1965) and thus quantify the relative sensitivity of the AN fiber to various tone frequencies. The stimulus used to measure the model tuning curves was a 50-ms tone followed by 50 ms of silence. The threshold is defined as the sound pressure level at which the average discharge rate during the 50-ms tone is 10 spikes/second greater than the average discharge rate dur-

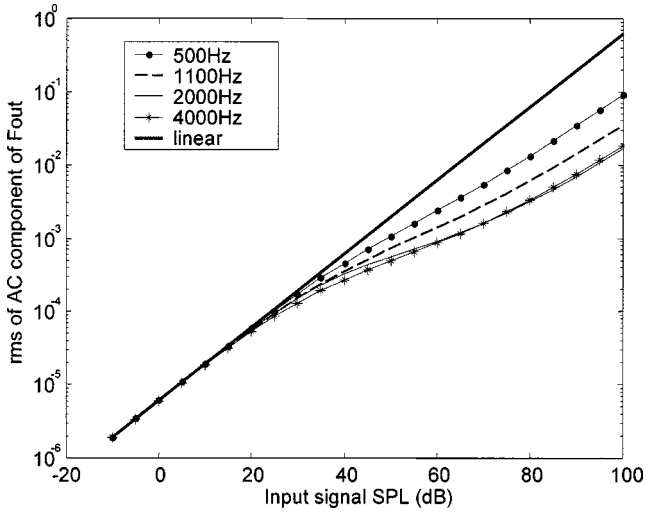

FIG. 7. The rms value of the signal path output, F_{out} (at steady state), in response to CF tones at different SPLs for model CFs at 500, 1100, 2000, and 4000 Hz, respectively. The response patterns demonstrate the compressive nonlinear nature of the signal path. The rms decreases as the model CF increases at a certain tone level, indicating a greater compression with higher CF.

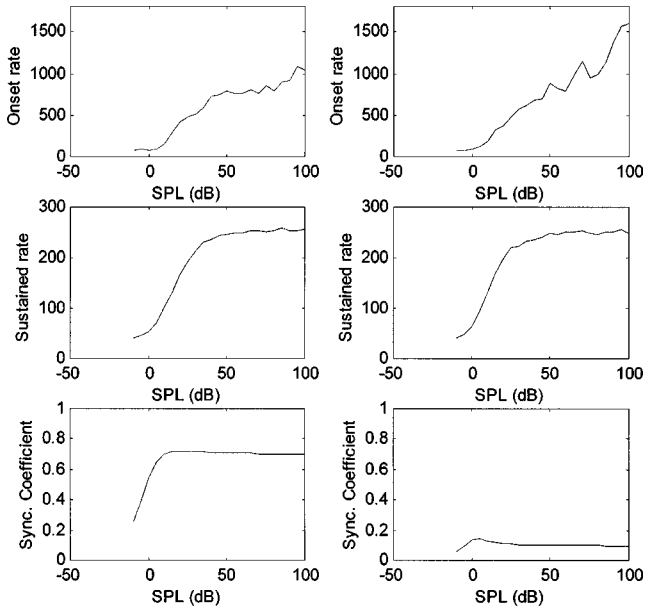

FIG. 8. Response rate and synchronization coefficient to CF-tone input with CF of 1100 Hz (left column) and 4000 Hz (right column). Onset rate is the maximum discharge rate during the first 10 ms and is calculated using 0.5-ms bins. The sustained rate and the synchronization coefficient were calculated in the 10- to 45-ms time window for 400 repetitions.

ing silence. Figure 9(a) shows tuning curves for the AN model at different CFs. The thresholds at CF were set between 0 and 10 dB by adjusting the gain in the IHC model. This threshold can also be adjusted by changing the gain in the middle-ear model. The width of model tuning curves depends on the bandwidth of the bandpass filter in the signal path. The model tuning curves lacks explicit ''tails'' on the low-frequency side as observed in physiological data (Kiang *et al.*, 1965; Kiang and Moxon, 1974; Liberman, 1978). However, this model is relatively sensitive to frequencies near subharmonics of CF due to the nonlinear filter in the signal path.

Q_{10} value (CF divided by the tuning-curve bandwidth 10 dB above threshold) is a standard measurement of the sharpness of tuning curves. The tuning of this AN model was adjusted to match model Q_{10} values to AN fibers with tuning sharper than 75% of the population data. Model Q_{10}'s, shown for a range of CFs in Fig. 9(b), were comparable to Q_{10} values measured from normal cat AN fibers (Miller *et al.*, 1997).

D. Reverse-correlation filters and level-dependence of BF

Threshold tuning curves provide a description of tuning in terms of changes in average discharge rate; however, reverse-correlation filters (the Fourier transform of the revcor function) provide a description of tuning that combines rate and temporal response properties. Figure 10 shows model and measured revcor filters based on noise responses across a range of sound levels. The peak of the revcor filter is an estimate of the fiber's BF, and shifts in the BF with level are seen for both measured [Fig. 10(a)] and model [Fig. 10(b)] revcor filters. The downward shift of BF as level increases is consistent with reports based on revcor filters (e.g., Evans,

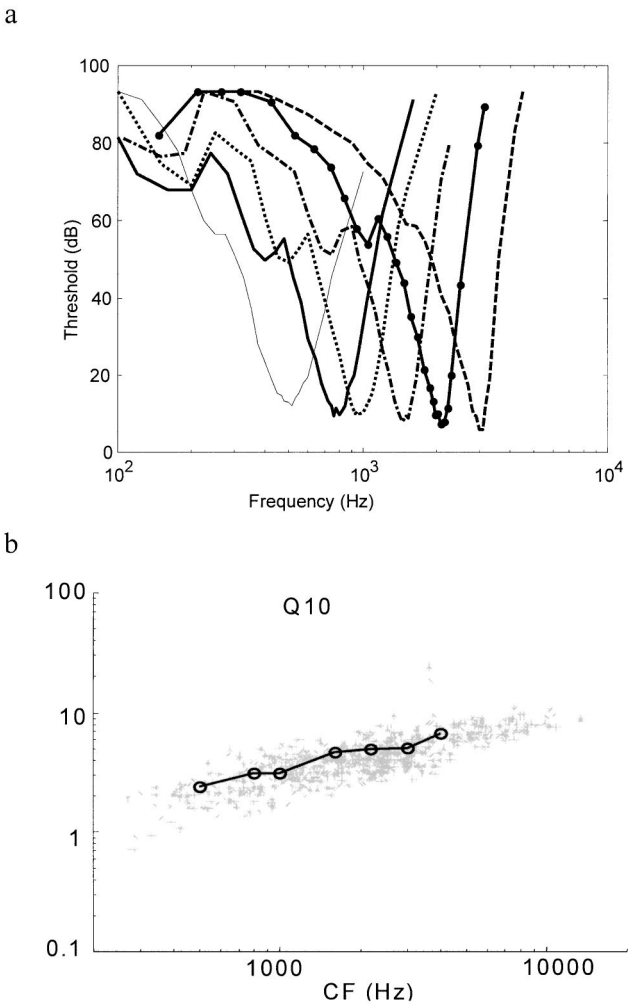

FIG. 9. (a) Model tuning curves for different CFs. The model threshold is defined as the pure-tone SPL that results in a rate response that is 10 spike/s greater than the spontaneous rate. (b) Q_{10} values measured from model tuning curves and compared with physiological data from Miller *et al.* (1997, their Fig. 3). Q_{10} data were used to set the locations of the poles of the bandpass filter in the signal path. Q_{10} values quantitatively described the sharpness of the model's tuning curves as a function of CF.

1977; Møller, 1977; de Boer and de Jongh, 1978) and with the level dependence of BM responses at high-CF places (e.g., Rhode, 1971; Ruggero *et al.*, 1997). As described above, this BF shift is also consistent with the level-independent upward instantaneous-frequency glide in the impulse responses of high-CF fibers. Low-CF fibers that have a downward glide have an upward shift in BF as level increases (not shown).

The shift in BF of the model AN fiber is less than that of the measured AN fiber [Figs. 10(a) and (b)]. This difference between the responses of the model and of this particular AN fiber suggests that they differ slightly either in the frequency range of the instantaneous-frequency glide and/or in the amount of compression, and thus in the temporal extent of the latency shifts as a function of level. The model parameters were based on the responses of a population of AN fibers and were not adjusted to match the responses of individual AN fiber examples.

In addition to the changes in BF and bandwidth that can be observed in the magnitudes of the revcor filters [Figs.

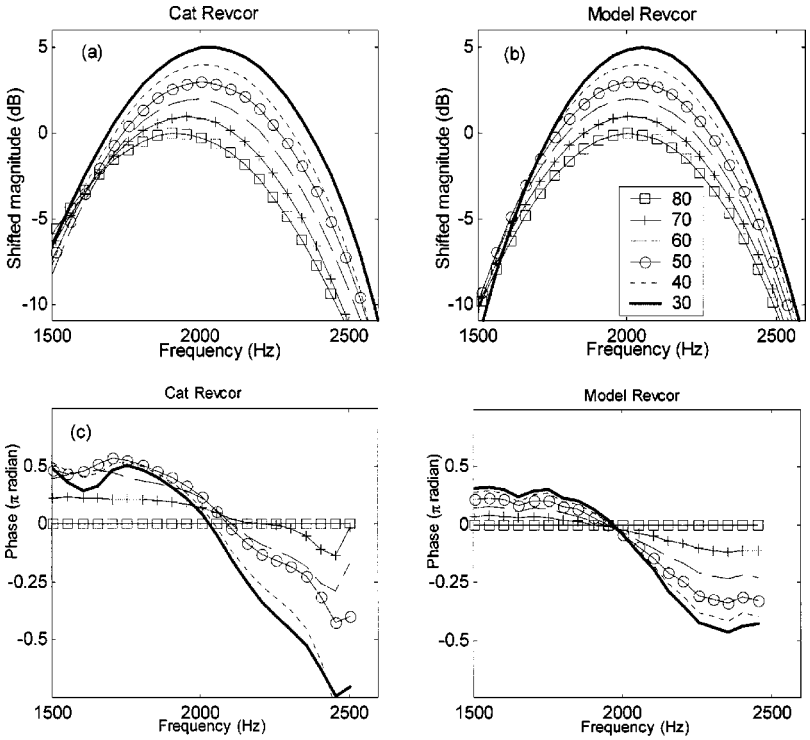

FIG. 10. Measured and model reverse-correlation filters. The top panels (a, c) show the magnitudes of the revcor filters computed in response to wideband noise at several stimulus levels. Each revcor filter was normalized by its peak magnitude; for clarity, a 1-dB shift was introduced between filters computed at different noise levels. The lower panels (b,d) show the level-dependent phases of the revcor filters, plotted relative to the phase at CF. The phases at CF were forced to be between $-\pi$ and $+\pi$. The measured AN responses are from unit 86100-25 from Carney and Yin (1988).

10(a) and (b)], the phases of the revcor filters change systematically with stimulus level [Figs. 10(c) and (d)]. As bandwidth increases at higher stimulus levels, the phase functions get shallower. These changes in bandwidth and phase are seen at both low and high CFs. The level-dependent phase properties of the revcor filters are consistent with the level dependence of phase-locked responses of AN fibers to tones (Anderson *et al.*, 1971). This property of the model was a focus of our modeling efforts because the level dependence of the timing of low-CF AN responses may be important for level coding at low frequencies (Carney, 1994; Heinz *et al.*, 2001b; Colburn *et al.*, 2003).

E. Response areas with phase responses

The upper panel of Fig. 11 shows a response area, or average discharge rates, for an AN model fiber (CF=2200 Hz) in response to tonal stimuli at several frequencies and levels. Each curve corresponds to responses to tones at a constant sound pressure level (iso-level contours). The peaks of the curves at low stimulus levels, or the center of gravity of the saturated responses at high stimulus levels, shift to lower frequencies as SPL increases; however, due to rate saturation, the shift in BF is not as apparent in the response area as it is in the revcor filter (Fig. 10). This BF shift is not seen in the Zhang *et al.* (2001) AN model (their Fig. 9) because the gammatone filter is essentially a symmetric filter in the frequency domain.

The frequency range over which this model responds at high stimulus levels is more limited here than for the Zhang *et al.* (2001) AN model. This narrower frequency range is more appropriate based on physiological descriptions of AN response areas (e.g., Anderson *et al.*, 1971). The difference in the models is due to the higher number of poles used in this model. This property of the higher-order filter can also be seen in the tuning curves (Fig. 9), which are narrower at higher levels for this model than for the Zhang *et al.*, (2001) model.

The lower panel of Fig. 11 shows the level-dependent phase shift for model fiber responses to pure tones with frequencies above and below model CF, referenced to the phase in response to tones at 90 dB SPL [following the plotting convention used in Anderson *et al.* (1971)]. Thus, any non-zero relative phase indicates that the response phase changes with level. The opposite phase change above and below CF is consistent with physiological data (Anderson *et al.*, 1971). However, the maximum negative phase change at frequen-

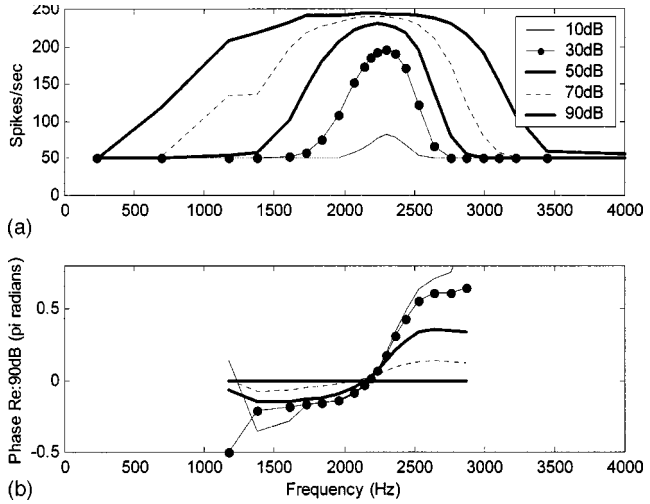

FIG. 11. Response area for model fiber with CF=2200 Hz. (a) Rate response (b) Phase response. Each line corresponds to an input tone SPL as indicated in the figure. The phase responses were referenced to the phase in response to that frequency at 90 dB SPL.

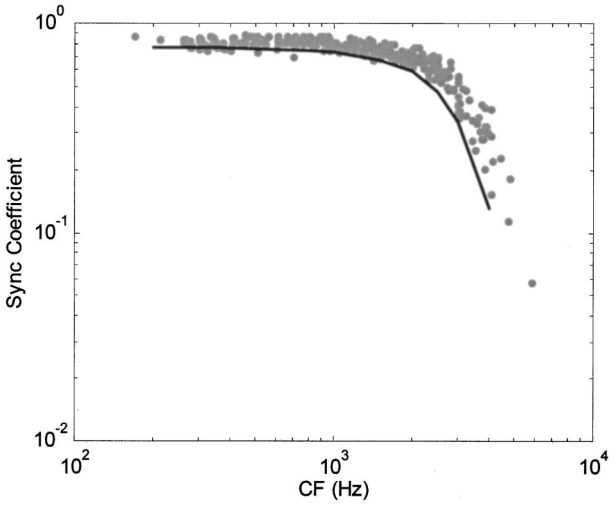

FIG. 12. Maximum synchronization coefficient. The results were measured by taking the maximum synchronization coefficient of model response to CF-tone inputs with SPLs from 0 to 100 dB (i.e., the maximum value from the curves in the bottom panels in Fig. 8). The stimuli were the same as in Fig. 8. Physiological data (Johnson, 1980) from a population of cat AN fibers are indicated with crosses.

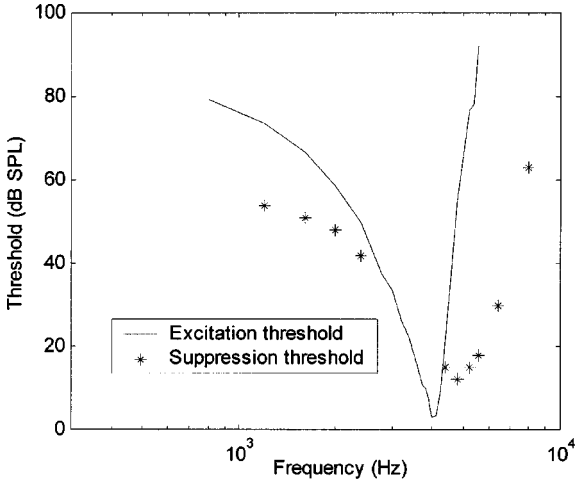

FIG. 13. Suppression threshold. The solid line illustrates the model's tuning curve with CF at 4000 Hz. The stars indicate the suppression threshold, which is defined as the suppressor tone SPL that decreases the response to CF tone by 10 spike/s.

cies below model CF is about $\pi/4$, which is smaller than the value of $\pi/2$ seen in AN fibers (Anderson *et al.*, 1971). This is a limitation of this model, as discussed below.

F. Synchronization coefficient of model AN fibers to CF tones as a function of CF

The synchronization coefficient measures how well the AN response is synchronized to the input pure tone in the time domain. A synchronization coefficient of one means that the AN response is perfectly phase-locked to the input pure tone. Figure 12 illustrates the maximum synchronization coefficient of this model's response to pure tones as a function of CF. The model response's synchronization is an important temporal property that indicates how well the AN response preserves the fine structure of input sound in the time domain. This ability of the AN model to phase lock to the fine structure of input sound is limited by the low-pass filtering in the IHC model. The parameters of the low-pass filter in the IHC and synapse model (Zhang *et al.*, 2001) were chosen to achieve the low-pass roll-off seen in AN data (Johnson, 1980). The model's synchronization coefficient (Fig. 12) is slightly smaller than that reported for cat (Johnson, 1980), due to the limitations of the synapse model. This limitation is also shown in Zhang *et al.* (2001), which has the same synapse model.

G. Two-tone suppression and suppression growth functions

Two-tone suppression (Nomoto *et al.*, 1964; Arthur *et al.*, 1970; Sachs and Kiang, 1968; Delgutte, 1990) is a nonlinear phenomenon of AN fiber responses, in which a stimulus away from CF can act to reduce the response to a stimulus near CF. Suppression was included in the AN model by making the bandwidth of the control path wider than that of the signal path, as suggested by Geisler and Sinex (1980). The suppressor passes through the relatively wideband control path and decreases the gain of the signal path. This feature is especially important for the simulation of AN responses to complex sounds, such as speech signals, where more than one frequency component is present. This suppression can be quantified by the suppression tuning curve (Fig. 13), which measures suppression threshold as a function of suppressor frequency. The suppression threshold is defined as the SPL of the suppressor when the response to a CF tone is reduced by ten spikes/second (Delgutte, 1990). The tips of suppression tuning curves are shifted toward the high-frequency side of excitatory tuning curves (Delgutte, 1990). To implement this tip shift, the center frequency of the wideband filter in the control path was set to be higher than the model CF. This selection of the wideband filter's center frequency (a higher value than CF) is also in agreement with the suggestion that the outer hair cells responsible for the nonlinearity at a given CF are located basally (i.e., tuned to a higher frequency) (Patuzzi, 1996).

While the suppression tuning curves describe the frequency tuning of the onset of suppression, it is also important to examine how suppression grows with level for frequencies above and below CF. The suppression growth function measures the amount of suppression at a particular suppressor frequency as a function of the SPL of the suppressor. The SPL of the CF tone was adjusted such that the response was constant as the suppressor SPL increased. Different slopes are shown for suppression growth functions at different suppressor frequencies for the same CF (Fig. 14): The suppressors with frequencies higher than CF show slower growth (shallower slope) than suppressors with frequencies below CF do. This asymmetrical growth in two-tone suppression has been observed in physiological experiments (Delgutte, 1990). For example, in Fig. 14 (CF=3500 Hz) the slope for growth of suppression by a 1550-Hz tone is 0.8 dB/dB, which is smaller than the averaged physiological data [about 1.3 for suppressor frequency/CF=0.44, Fig. 9 of Delgutte (1990)]. The slope for growth of suppression by a 4400-Hz tone is 0.4 dB/dB, which agrees with the slope

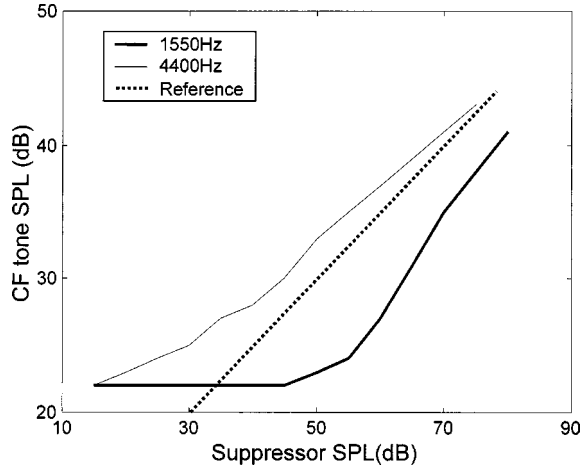

FIG. 14. Suppression growth functions measured for a CF of 3500 Hz, with suppressors at 1550 Hz (below CF) or 4400 Hz (above CF). The CF tone SPL was adjusted to maintain a response rate that was two-thirds of the maximum response rate at each suppressor SPL. The dotted line indicates a growth with slope of 1 (dB/dB).

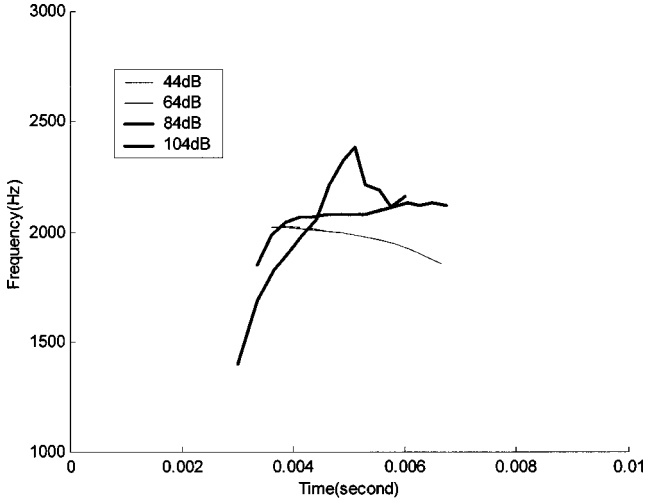

FIG. 15. Instantaneous frequencies calculated for the DRNL model (Meddis *et al.*, 2001) impulse responses for a CF of 2000 Hz at different sound pressure levels (40 to 100 dB in 20-dB steps) based on the zero-crossing method (see Appendix B). A level dependency in the instantaneous profile is demonstrated by the changes in the direction of the glides at different levels. Note that the instantaneous profiles for the two lowest levels are nearly identical, so the curves lie atop one another.

observed physiologically for a suppressor frequency 1.26 times CF (Delgutte, 1990).

IV. DISCUSSION

This report describes a computational AN model that has a level-independent frequency glide and nonlinear compression. AN models based on gamma-tone filters (Carney, 1993; Zhang *et al.*, 2001) do not have frequency glides in their impulse responses because the frequency response of the gamma-tone filter is symmetrical. Pfeiffer's (1970) BPNL model and its extension, Goldstein's (1990, 1995) MBNL model, did not address the level independence of the instantaneous-frequency glide. Meddis *et al.* (2001) qualitatively described the frequency glide in their model's impulse responses, but they did not quantify this response property or examine its level dependence. We explored the level dependence of the frequency glide in the DRNL model by producing impulse responses for a 2000-Hz CF fiber at several input sound pressure levels and calculating the corresponding instantaneous frequencies as a function of time (Fig. 15). Because the DRNL model achieves its changes in bandwidth by changing the overall shape (and thus symmetry) of its frequency response with level, we anticipated that the instantaneous-frequency glide of this model would be level dependent. Indeed, the instantaneous-frequency profile of the DRNL model changes considerably as a function of level (Fig. 15), which is inconsistent with the level-independent frequency glide reported for AN fibers [e.g., Fig. 3 in Carney *et al.* (1999), and cf. Fig. 6 for the model presented here]. The instantaneous frequency of the DRNL model has the same downward glide at the two lowest levels tested (44 and 64 dB SPL) and has an upward frequency glide at higher SPLs.

Irino and Patterson (2001) demonstrated an instantaneous-frequency glide in the impulse response of their gammachirp-based model. However, the trend of this model's best-frequency shift, which is a feature associated with the frequency glide in the impulse response, is not consistent with physiological results. In Fig. 7 of Irino and Patterson (2001), best frequency (CF=2000 Hz) first shifts to a relatively higher frequency and then shifts down as the input SPL increases from 30 to 80 dB. In Fig. 10 of Irino and Patterson (2001), the best frequency increases as the input SPL changes from 30 to 60 dB. However, Anderson *et al.* (1971, their Fig. 8) and Møller (1977) show that the best frequency in responses of AN fibers with mid- to high-frequency CFs shifts to lower frequencies as the input SPL increases. The best-frequency shift can be qualitatively explained by the interaction between the instantaneous frequency glide in the impulse response and the change in the shape of the impulse response envelope at various input SPLs due to the compressive nonlinearity (Carney, 1999). The monotonicity of the IF profiles of the impulse response is also consistent with the monotonic BF shifts that have been observed as a function of SPL.

A. Limitations and future work

The goal of this study was to provide a computational phenomenological AN model with more complete response features than those of previous AN models, and efforts focused on modeling the level-independent frequency glide. The instantaneous frequency glide and compressive nonlinearity were successfully included in this model. This model does have some limitations, however. Only AN fibers with high spontaneous rate have been implemented to date; other spontaneous rate fibers will be considered in future work. The major changes related to modeling low and medium spontaneous rate fibers would be mostly within the IHC and synapse model, and it is anticipated that the configuration of the signal path and the control path described here will not be changed.

The values of this model's parameters were estimated on the basis of revcor functions recorded from low-frequency AN fibers (Carney *et al.*, 1999, below 4000 Hz), which limits

the application of this model in processing signals with relatively high frequency components. Revcor data based on BM measurements are available for higher CFs (de Boer and Nuttall, 1997). These BM revcor data could be used for parameter estimation at high CFs by calculating model revcor functions from the signal path output and then fitting these model revcor functions to BM data.

Another limitation is the relatively small phase shift below CF in the intensity-dependent phase responses (Fig. 11). The limited phase shift is due to the limited number of poles in the signal-path filter and may also be due to the level independence of the zeros' locations. These limitations can be overcome with a more complicated AN model; however, the results presented here focused on a relatively simple model structure.

A primary motivation for the development of this model was to provide a tool for understanding the implications of the frequency glide for stimulus coding. The glide is level independent, but because it interacts with the compressive nonlinearity, its influence on the rate and timing of AN responses is complex. Using techniques that have been developed in recent studies (e.g., Heinz *et al.*, 2001a,b, 2002; Tan, 2003), this computational AN model can be used in future studies to explore the implications of the frequency glide for predictions based on AN responses of psychophysical performance on basic tasks. This model can also be applied to studies of AN responses to more complex stimuli, such as speech sounds (e.g., Bruce, 2003). Tan (2003) has recently applied this AN model to a study of the coding of vowel-like stimuli, including predicting the limits of psychophysical performance in formant-frequency discrimination in quiet and in noise based on population AN responses.

ACKNOWLEDGMENTS

We acknowledge the helpful comments and suggestions of Michael Heinz, Susan Early, Xuedong Zhang, Ian Bruce, Satish Iyengar and Jayant Datta. This work is supported by Grant No. IBN-9983567 from the National Science Foundation and Grant No. DC01641 from the National Institutes of Health. Dr. Christopher Plack kindly provided the computer code for the DRNL model. Dr. Don Johnson generously provided the synchronization coefficient data for AN fibers. Dr. Roger Miller generously provided the Q_{10} data for AN fibers.

APPENDIX A: EXAMPLES OF CF-DEPENDENT PARAMETER VALUES FOR THREE CFS

CF (Hz)	500	1000	2200	Description
σ (rad/s)	954	1258.9	1725.7	Real part of the pole closest to the imaginary axis
P_ω (rad/s)	436.7	979.4	2281.9	Imaginary part of the pole closest to the imaginary axis
P_a (rad/s)	835.1	1697.1	3801.9	Relative locations of poles in signal path, real part
P_b(rad/s)	−496	357.1	3187.8	Relative locations of poles in signal path, imaginary part
X_{zero} (rad/s)	1407.5	3981	12990	The distance from the origin to the zeroes along the negative real axis
G_{control}	650.1	1445.6	3023.8	Gain in control path

APPENDIX B: CALCULATION OF INSTANTANEOUS FREQUENCY

Two methods can be used to calculate the instantaneous frequency of a model or data revcor function, $s(t)$. The first method was based on the Hilbert transform. A complex signal is made by taking $s(t)$ as the real part and the Hilbert transform of $s(t)$ as the imaginary part. The time-domain derivative of the phase of this complex signal is the instantaneous frequency of the revcor function s(t). The second method was based on identifying the zero-crossing points in the revcor functions. The instantaneous frequency of the impulse response was estimated as the reciprocal of the instantaneous period, which is equal to two times the distance between sequential zero crossings.

Before estimating the instantaneous frequency with either method, a three-point average of the original revcor function was performed to smooth the revcor function. Also, the instantaneous frequency profile was only estimated over a time interval for which the envelope amplitude was at least 25% of the maximum value (de Boer and Nuttall, 1997), which avoided noisy fluctuations where the revcor function amplitude was too small to make accurate estimates. In general, these two methods gave similar results; however, the method based on the Hilbert transform was more sensitive to noise in the revcor function and therefore showed more oscillation in the results. The results presented in Figs. 6 and 14 are therefore based on the zero-crossing method.

[1]Best frequency (BF) is the frequency at which the fiber response is strongest at a certain SPL (peak frequency of the response area curve, see Fig. 10). The characteristic frequency (CF) is the frequency at which the threshold of the fiber is lowest.

[2]The C code used to implement this model is available at http://earlab.bu.edu

[3]To get real responses in the time domain after the inverse Laplace transform, poles were arranged in conjugate pairs in the Laplace domain.

Anderson, D. J., Rose, J. E., Hind, J. E., and Brugge, J. F. (**1971**). "Temporal position of discharges in single auditory nerve fibers within the cycle of a sine-wave stimulus: Frequency and intensity effects," J. Acoust. Soc. Am. **49**, 1131–1139.

Arthur, M. A., Pfeiffer, R. R., and Suga, N. (**1970**). "Properties of 'two-tone inhibition' in primary auditory neurons," J. Physiol. **212**, 593–1139.

Bruce, I. C., Sachs, M. B., and Young, E. D. (**2003**). "An auditory-periphery model of the effects of acoustic trauma on auditory nerve responses," J. Acoust. Soc. Am. **113**, 369–388.

Carney, L. H. (**1993**). "A model for the responses of low-frequency auditory nerve fibers in cat," J. Acoust. Soc. Am. **93**, 401–417.

Carney, L. H. (**1994**). "Spatiotemporal encoding of sound level: Models for normal encoding and recruitment of loudness," Hear. Res. **76**, 31–44.

Carney, L. H. (**1999**). "Temporal response properties of neurons in the auditory pathway," Curr. Opin. Neurobiol. **9**, 442–446.

Carney, L. H., and Yin, T. C. T. (**1988**). "Temporal coding of resonances by low-frequency auditory nerve fibers: Single fiber responses and a population model," J. Neurophysiol. **60**, 1653–1677.

Carney, L. H., McDuffy, M. J., and Shekhter, I. (**1999**). ''Frequency glides in the impulse responses of auditory-nerve fibers,'' J. Acoust. Soc. Am. **105**, 2384–2391.
Cheatham, M. A., and Dallos, P. (**1999**). ''Response phase: A view from the inner hair cell,'' J. Acoust. Soc. Am. **105**, 799–810.
Cheatham, M. A., and Dallos, P. (**2001**). ''Inner hair cell response patterns: implications for low-frequency hearing,'' J. Acoust. Soc. Am. **110**, 2034–2044.
Colburn, H. S., Carney, L. H., and Heinz, M. G. (**2003, in press**). ''Quantifying the information in auditory-nerve responses for level discrimination,'' JARO.
de Boer, E. (**1997**). ''Connecting frequency selectivity and nonlinearity for models of the cochlea,'' Aud. Neurosci. **3**, 377–388.
de Boer, E., and de Jongh, H. R. (**1978**). ''On cochlear encoding: Potentialities and limitations of the reverse-correlation technique,'' J. Acoust. Soc. Am. **63**, 115–135.
de Boer, E., and Nuttall, A. L. (**1997**). ''The mechanical waveform of the basilar membrane. I. Frequency modulations (glides) in impulse responses and cross-correlation functions,'' J. Acoust. Soc. Am. **101**, 3583–3592.
de Boer, E., and Nuttall, A. L. (**2000**). ''The mechanical waveform of the basilar membrane. III. Intensity effects,'' J. Acoust. Soc. Am. **107**, 1497–1507.
Delgutte, B. (**1990**). ''Two-tone rate suppression in auditory-nerve fibers: Dependence on suppressor frequency and level,'' Hear. Res. **49**, 225–246.
Evans, E. F. (**1977**). ''Frequency selectivity at high signal levels of single units in cochlear nerve and nucleus,'' in *Psychophysics and Physiology of Hearing*, edited by E. F. Evans and J. P. Wilson (Academic, London), pp. 185–192.
Geisler, C. D., and Sinex, D. G. (**1980**). ''Responses of primary auditory fibers to combined noise and tonal stimuli,'' Hear. Res. **3**, 317–334.
Goldstein, J. L. (**1990**). ''Modeling rapid wave form compression on the basilar membrane as multiple-band-pass-nonlinearity filtering,'' Hear. Res. **49**, 39–60.
Goldstein, J. L. (**1995**). ''Relations among compression, suppression, and combination tones in mechanical responses of the basilar membrane: data and MBPNL model,'' Hear. Res. **89**, 52–68.
Heinz, M. G., Colburn, H. S., and Carney, L. H. (**2001a**). ''Evaluating auditory performance limits: I. One-parameter discrimination using a computational model for the auditory nerve,'' Neural Comput. **13**, 2273–2316.
Heinz, M. G., Colburn, H. S., and Carney, L. H. (**2001b**). ''Rate and timing cues associated with the cochlear amplifier: Level discrimination based on Monaural cross-frequency concidence detection,'' J. Acoust. Soc. Am. **110**, 2065–2084.
Heinz, M. G., Colburn, H. S., and Carney, L. H. (**2002**). ''Quantifying the implications of nonlinear cochlear tuning for auditory-filter estimates,'' J. Acoust. Soc. Am. **111**, 996–1011.
Heinz, M. G., Zhang, X., Bruce, I. C., and Carney, L. H. (**2001c**). ''Auditory-nerve model for predicting performance limits of normal and impaired listeners,'' ARLO **2**, 91–96.
Irino, T., and Patterson, R. D. (**1997**). ''A time-domain, level-dependent auditory filter: the gammachirp,'' J. Acoust. Soc. Am. **101**, 412–419.
Irino, T., and Patterson, R. D. (**2001**). ''A compressive gammachirp auditory filter for both physiological and psychophysical data,'' J. Acoust. Soc. Am. **109**, 2008–2022.
Johnson, D. H. (**1980**). ''The relationship between spike rate and synchrony in responses of auditory-nerve fibers to single tones,'' J. Acoust. Soc. Am. **68**, 1115–1122.
Kiang, N. Y. S., and Moxon, E. C. (**1974**). ''Tails of tuning curves of auditory-nerve fibers,'' J. Acoust. Soc. Am. **55**, 620–630.
Kiang, N. Y. S., Watanabe, T., Thomas, E. C., and Clark, L. F. (**1965**). ''Discharge patterns of single fibers in the cat's auditory nerve,'' MIT Research Monograph No. 35 (MIT, Cambridge, MA).
Liberman, M. C. (**1978**). ''Auditory-nerve responses from cats raised in a low-noise chamber,'' J. Acoust. Soc. Am. **63**, 442–455.
Lin, T., and Guinan, J. J. (**2000**). ''Auditory-nerve-fiber responses to high-level clicks: Interference patterns indicate that excitation is due to the combination of multiple drives,'' J. Acoust. Soc. Am. **107**, 2615–2630.
Marquardt, D. W. (**1963**). ''An Algorithm for Least-Squares Estimation of Nonlinear Parameters,'' J. Soc. Ind. Appl. Math. **11**, 431–441.
Meddis, R., O'Mard, L. P., and Lopez-Poveda, E. A. (**2001**). ''A computational algorithm for computing nonlinear auditory frequency selectivity,'' J. Acoust. Soc. Am. **109**, 2852–2861.
Miller, R. L., Schilling, J. R., Franck, K. R., and Young, E. D. (**1997**). ''Effects of acoustic trauma on the representation of the vowel /ɛ/ in cat auditory nerve fibers,'' J. Acoust. Soc. Am. **101**, 3602–3616.
Møller, A. R. (**1977**). ''Frequency selectivity of single auditory-nerve fibers in response to broadband noise stimuli,'' J. Acoust. Soc. Am. **62**, 135–142.
Mountain, D. C., and Hubbard, A. E. (**1996**). ''Computational analysis of hair cell and auditory nerve processes,'' in *Auditory Computation*, edited by H. L. Hawkins, T. A. McMullen, A. N. Popper, and R. R. Fay (Springer-Verlag, New York), pp. 121–156.
Nomoto, M., Suga, N., and Katsuki, Y. (**1964**). ''Discharge pattern and inhibition of primary auditory nerve fibers in the monkey,'' J. Neurophysiol. **27**, 768–787.
Patuzzi, R. (**1996**). ''Cochlear micromechanics and macromechanics,'' in *The Cochlea*, edited by P. Dallos, A. N. Popper, and R. R. Fay (Springer-Verlag, New York), pp. 186–257.
Pfeiffer, R. R. (**1970**). ''A model for two-tone inhibition of single cochlear-nerve fibers,'' J. Acoust. Soc. Am. **48**, 1373.
Recio, A., Narayan, S. S., and Ruggero, M. A. (**1997**). ''Wiener-kernel analysis of basilar membrane response to noise,'' in *Diversity in Auditory Mechanics*, edited by E. R. Lewis, G. R. Long, R. F. Lyon, P. M. Narins, C. R. Steele, and E. Hecht-Poinar (World Scientific, Singapore), pp. 325–331.
Recio, A., Narayan, S. S., and Ruggero, M. A. (**1998**). ''Basilar-membrane responses to clicks at the base of the chinchilla cochlea,'' J. Acoust. Soc. Am. **103**, 1972–1989.
Rhode, W. S. (**1971**). ''Observations of the vibration of the basilar membrane in squirrel monkeys using the Mossbauer technique,'' J. Acoust. Soc. Am. **49**, 1218–1231.
Rhode, W. S., and Cooper, N. P. (**1996**). ''Nonlinear mechanics in the apical turn of the chinchilla,'' Aud. Neurosci. **3**, 101–120.
Robert, A., and Eriksson, J. L. (**1999**). ''A composite model of the auditory periphery for simulating responses to complex sounds,'' J. Acoust. Soc. Am. **106**, 1852–1864.
Robles, L., Rhode, W. S., and Geisler, C. D. (**1976**). ''Transient response of the basilar membrane measured in squirrel monkeys using the Mossbauer effect,'' J. Acoust. Soc. Am. **59**, 926–939.
Rosowski, J. J. (**1996**). ''Models of External- and Middle-Ear Function,'' in *Auditory Computation*, edited by H. L. Hawkins, T. A. McMullen, A. N. Popper, and R. R. Fay (Springer-Verlag, New York), pp. 15–61.
Ruggero, M. A., and Rich, N. C. (**1991**). ''Furosemide alters organ of corti mechanics: evidence for feedback of outer hair cells upon the basilar membrane,'' J. Neurosci. **11**, 1057–1067.
Ruggero, M. A., Rich, N. C., Recio, A., Narayan, S. S., and Robles, L. (**1997**). ''Basilar-membrane responses to tones at the base of the chinchilla cochlea,'' J. Acoust. Soc. Am. **101**, 2151–2163.
Sachs, M. B., and Kiang, N. Y. S. (**1968**). ''Two-tone inhibition in auditory-nerve fibers,'' J. Acoust. Soc. Am. **43**, 1120–1128.
Shekhter, I., and Carney, L. H. (**1997**). ''A nonlinear auditory nerve model for CF-dependent shifts in tuning with sound level,'' Assoc. Res. Otolaryngol. **20**, 617.
Shera, C. A. (**2001a**). ''Frequency glides in click responses of the basilar membrane and auditory nerve: Their scaling behavior and origin in traveling-wave dispersion,'' J. Acoust. Soc. Am. **109**, 2023–2034.
Shera, C. A. (**2001b**). ''Intensity-invariance of fine time structure in basilar-membrane click responses: Implications for cochlear mechanics,'' J. Acoust. Soc. Am. **110**, 332–348.
Smith, R. L. (**1988**). ''Encoding of sound intensity by auditory neurons,'' in *Auditory Function: Neurobiological Bases of Hearing*, edited by G. M. Edelman, W. E. Gall, and W. M. Cowan (Wiley, New York), pp. 243–274.
Tan, Q. (**2003**). ''Computational and statistical analysis of auditory peripheral processing for vowel-like signals,'' Ph.D. dissertation, Boston University.
Tan, Q., and Carney, L. H. (**1999**). ''A phenomenological model for auditory nerve responses: Including the frequency glide in the impulse response,'' Proc. IEEE 25th Annual Northeast Bioengineering Conference, pp. 23–24.
Westerman, L. A., and Smith, R. L. (**1988**). ''A diffusion model of the transient response of the cochlear inner hair cell synapse,'' J. Acoust. Soc. Am. **83**, 2266–2276.
Zhang, X., Heinz, M. G., Bruce, I. C., and Carney, L. H. (**2001**). ''A phenomenological model for the responses of auditory-nerve fibers. I. Nonlinear tuning with compression and suppression,'' J. Acoust. Soc. Am. **109**, 648–670.